Available online at www.sciencedirect.com

ScienceDirect

Energy Procedia 97 (2016) 67 – 74

Energy Procedia

European Geosciences Union General Assembly 2016, EGU
Division Energy, Resources & Environment, ERE

Water and CO_2 permeability of a shale sample core from Svalbard

Reinier van Noort[a]*, Viktoriya Yarushina[a]

[a]*Institute for Energy Technology (IFE), Department for Environmental Technology, Kjeller 2055, Norway.*

Abstract

Flow in tight shales is thought to be largely confined to fractures and similar features. Therefore, how open such features are under in-situ conditions has a major impact on shale permeability. We performed 43 permeability measurements on one shale core sample, both when it was intact and after it had fractured, using either water or supercritical CO_2 as the permeate. Our measurements show decreasing permeability with increasing confining pressure, due to both instantaneous and time-dependent, permanent compaction. Furthermore, our measurements show that under confinement, compaction may also eliminate the effect of a simple splitting fracture on shale permeability.

Peer-review under responsibility of the organizing committee of the General Assembly of the European Geosciences Union (EGU)

Keywords: shale; pressure-dependent permeability; fluid flow; fracture flow; creep; CO_2

1. Introduction

In many geo-engineering practices, shales play an important role, as shale can act as source rock, caprock, or even reservoir rock. As a source rock, shale allows hydrocarbon-rich fluids to escape, whereas as a caprock shale forms a barrier to fluid flow. Hydraulic fracturing is often required to enhance fluid flow when producing hydrocarbons from shale reservoirs. The overlying caprock above many reservoirs targeted for CO_2-injection is shale.

* Corresponding author. Tel.: +4792430032.
E-mail address: reinier@ife.no

Peer-review under responsibility of the organizing committee of the General Assembly of the European Geosciences Union (EGU)
doi:10.1016/j.egypro.2016.10.021

Previous experimental work has shown that shale permeability strongly depends on the applied effective confining pressure [1,2], as shale deforms elastically, plastically and by time-dependent viscous deformation [3]. Models suggest that due to shale deformability and the pressure-sensitivity of shale permeability, significant fluid fluxes are possible in shales (e.g., [4,5]). This is supported by laboratory experiments [6] and seismic observations indicating localized channels of increased fluid flow fluxes cutting through shales [7]. Therefore, it is of great importance to properly understand the flow of fluids through shale, as well as the possible interactions between shale and fluid that may influence this flow (i.e., mechanical effects, chemical effects [8,9], and swelling or shrinkage of clay minerals [10–12]).

To better understand fluid flow mechanisms in shales under in-situ stress conditions, we performed 43 permeability measurements on a single confined shale core plug from borehole DH7A in the Longyearbyen CO_2 well park in Adventdalen, on Svalbard's main island Spitsbergen on the northwestern margin of the Barents Sea Shelf [13]. These measurements have been carried out using either water or supercritical CO_2 as the permeate, to allow a comparison between water- and CO_2-permeability, under an effective isotropic confining pressure approximating sub-surface conditions relevant for CO_2-storage.

2. Method

2.1. Sample

The sample plug tested was drilled from a core that was retrieved on 23-06-2012 from borehole DH7A, from a depth of 375.25-375.47 m. Considering this depth and location, the sample originated from the Rurikfjellet formation (cf., [13]). Based on XRD analyses [14] on samples from borehole DH4, which was drilled in the same location, less than 100 m away, the main mineral phases present in our sample are illite, with only minor interlayered smectite, quartz, and plagioclase, with minor carbonates, kaolinite, and Fe-chlorite. The sample plug was drilled parallel to bedding, while keeping the shale under compression to prevent cracking. The core plug had a diameter of 25 mm and a thickness of 10 mm.

2.2. Apparatus and experimental method

All measurements reported here were carried out in a purpose-built transient pulse permeability apparatus, using a technique similar to that described in [15–17]. In our apparatus, a 25 mm diameter cylindrical sample is stacked between two hastelloy microporous plates, and two hastelloy pistons with grooved surfaces (to improve fluid flow distribution), and jacketed in a heat-shrink Fluorinated Ethylene Propylene (FEP) jacket, sealed to the pistons with steel wire tourniquets. For measurements performed with CO_2 as the pore fluid, aluminum foil is wrapped around the sample and pistons before sealing the assembly in its FEP jacket, as CO_2 diffuses through the FEP. The sample assembly is then placed inside a confining vessel, and the two pistons are each connected to an accurately calibrated volume. The confining pressure is applied using water as the confining medium. During the experiments performed at 40 °C, a temperature stability better than ± 0.1 °C is achieved by placing the apparatus inside a temperature-controlled cabinet (Termaks TS 8136), using an incandescent light bulb connected to a thyristor for precision control. The pore fluid pressure is maintained using an ISCO 100DX volumetric pump. Data is recorded at regular intervals (usually at 0.1 Hz) using an Agilent 34970A data acquisition/switch unit data logger connected to a PC. Data logs include temperature (K-type thermocouples), measured both inside the pressure vessel close to the sample, and in the temperature-controlled cabinet, pump pressure, pump piston position, and up- and downstream pore pressures and confining pressure (Unik 5000 pressure sensors with a range of 0-70 MPa and an accuracy of 0.1 % of full scale).

When setting up a series of measurements, the confining and pore fluid pressures are increased stepwise, such that the effective confining pressure is always kept below the desired value for the first measurement. Then, once the sample is stabilized at the desired confining and downstream pressures, a measurement is started by briefly opening the valve between the upstream volume and the ISCO pump, increasing the upstream pressure by 0.2 MPa. Once the valve is closed, pulse decay is monitored. Between measurements, the sample was kept under pressure.

During our experiments, the sample jacket had to be replaced three times due to system leakages. Furthermore, the jacket had to be replaced to add an aluminum foil layer when measurements with CO_2 were started. Before these measurements, the sample was flushed with supercritical CO_2, and air-dried to remove pore water and prevent two-phase flow effects. During the first jacket replacement, i.e., between the first and second measurement series, the sample fractured along a plane parallel to its bedding and the sample axis. Fig. 1 shows a photo of the core plug after it had split. Hence, all measurements after that were performed on this fractured sample.

2.3. Data treatment

Except when permeabilities are high, and therefore pressure changes are rapid, to reduce noise, all up- and downstream pressure datasets are first smoothed using a variable moving average routine. Typically, this smoothing was done over a pressure change of 2.5% of the applied pulse. Next, volumetric flowrates (Q) are calculated from the smoothed up- and downstream pressures and fluid densities are calculated using the FLUIDCAL software [18], and from this the permeability can be calculated, using the Darcy flow law:

$$-\kappa = \frac{Q\mu L}{A(P_H - P_L)}$$

P_H and P_L are, respectively, the up- and downstream pressures. Fluid viscosities (μ) are calculated using the FLUIDCAL software. Variables L and A are the sample length and the sample surface area through which flow takes place. They are assumed to be constant, and independent of effective confining pressure (i.e., we assumed that while compaction may have significant effects on permeability, changes in the sample dimensions are negligible for the purpose of these calculations). Permeabilities are then calculated for each data point over a set change in pressure around that data point, as was done in smoothing, typically 5% of the total pressure pulse, to further cancel out noise effects.

3. Results

A list of all permeabilities measured, along with measurement conditions, is given in Table 1. The data is divided into 5 series of measurements, corresponding to experiments performed between each replacement of the sample jacket, and hence depressurization of the sample. All permeability measurements are plotted against effective confining pressure in fig. 2.

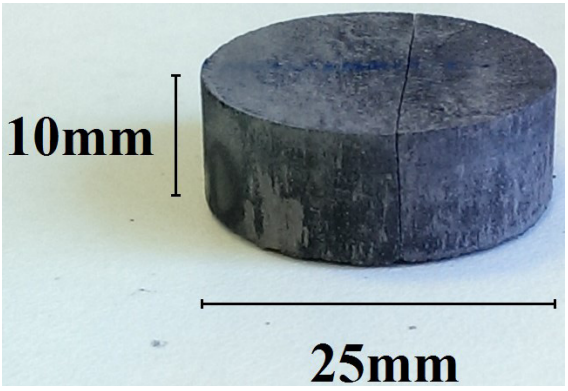

Fig. 1. The shale core plug split along its bedding, parallel to the sample axis.

Table 1. Experimental PT-conditions, and measured permeabilities.

Measurement no.	Notes	P conf. (MPa)	Initial pore P (MPa)	Effective P conf. (MPa)	T (°C)	Permeability (m^2)
1-40272501	Intact core, permeate water	4	2.5	1.4	RT	6.6×10^{-18}
1-80272501		8	2.5	5.4	RT	7.9×10^{-19}
1-80272502		8	2.5	5.4	RT	8.6×10^{-19}
1-80272503		8	2.5	5.4	RT	9.3×10^{-19}
1-80272504		8	2.5	5.4	RT	8.5×10^{-19}
1-100272501		10	2.5	7.4	RT	4.0×10^{-19}
1-100272502		10	2.5	7.4	RT	3.9×10^{-19}
1-100272503		10	2.5	7.4	RT	3.7×10^{-19}
1-1502725b03		15	2.5	12.4	RT	1.5×10^{-19}
1-1502725b04		15	2.5	12.4	RT	1.5×10^{-19}
1-1502725b05		15	2.5	12.4	RT	1.6×10^{-19}
1-1002725b02		10	2.5	7.4	RT	9.9×10^{-20}
1-802725c01		8	2.5	5.4	RT	1.1×10^{-19}
1-502725c04		5	2.5	2.4	RT	9.5×10^{-20}
1-502725c05		5	2.5	2.4	RT	9.2×10^{-20}
1-1002725d01		10	2.5	7.4	RT	6.1×10^{-20}
1-1002725d02		10	2.5	7.4	RT	6.3×10^{-20}
1-1502725d01		15	2.5	12.4	RT	4.5×10^{-20}
1-1502725d02		15	2.5	12.4	RT	4.6×10^{-20}
1-2002725a01		20	2.5	17.4	RT	2.7×10^{-20}
1-2002725b02		20	2.5	17.4	RT	2.5×10^{-20}
1-2002725b03		20	2.5	17.4	RT	2.4×10^{-20}
2-502725x01	Fractured core, permeate water	5	2.5	2.4	RT	1.9×10^{-19}
2-502725x02		5	2.5	2.4	RT	1.9×10^{-19}
2-502725x03		5	2.5	2.4	RT	1.7×10^{-19}
2-2002725x01		20	2.5	17.4	RT	8.0×10^{-21}
2-2002725x02		20	2.5	17.4	RT	5.9×10^{-21}
2-4002725a01		40	2.5	37.4	RT	2.0×10^{-21}
3-1255250x02	Fractured core, permeate water	12.5	5	7.4	40	1.9×10^{-21}
3-12552c50x05		12.5	5	7.4	40	9.6×10^{-22}
3-1255250x06		12.5	5	7.4	40	2.3×10^{-21}
3-2255250 01		22.5	5	17.4	40	1.3×10^{-21}
3-2255250 02		22.5	5	17.4	40	1.1×10^{-21}
4-2255250e03	Fractured core, permeate water	22.5	5	17.4	40	3.6×10^{-21}
4-2255250e04		22.5	5	17.4	40	3.6×10^{-21}
4-2255250e05		22.5	5	17.4	40	3.8×10^{-21}
4-2255250e06		22.5	5	17.4	40	3.2×10^{-21}
4-2255250e07		22.5	5	17.4	40	3.4×10^{-21}
4-2507775a01		25	7.5	17.4	40	3.8×10^{-21}
4-2507775a02		25	7.5	17.4	40	4.0×10^{-21}
5-2507775CO202	Fractured core, permeate $scCO_2$	25	7.5	17.4	40	1.6×10^{-21}
5-2507775CO203		25	7.5	17.4	40	3.2×10^{-21}
5-2507775CO204		25	7.5	17.4	40	1.4×10^{-21}

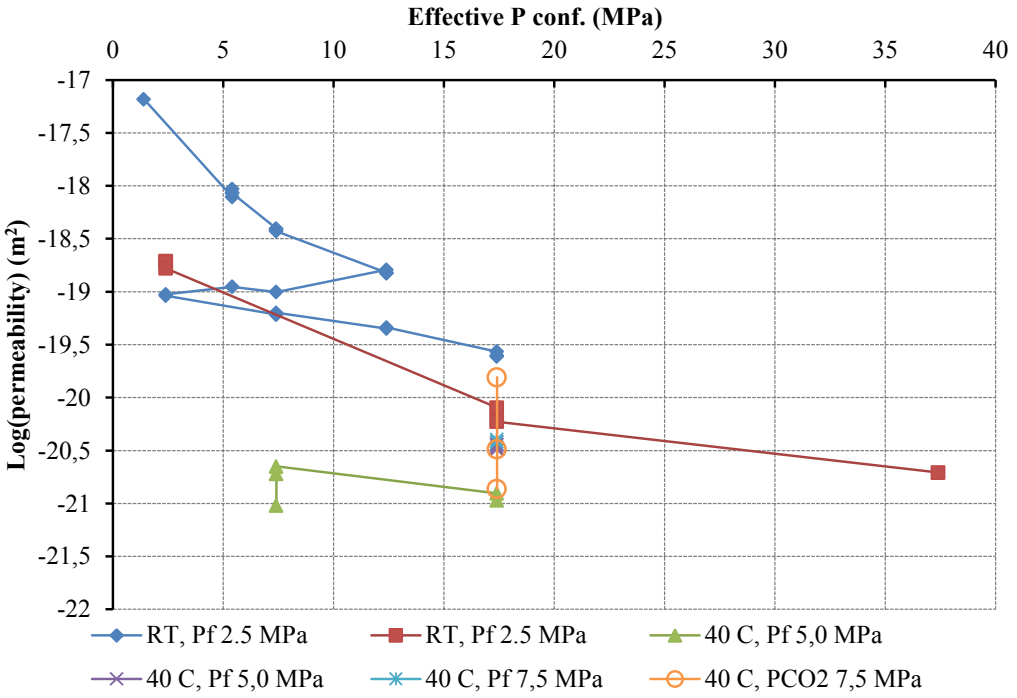

Fig. 2. All permeability measurements plotted against effective confining pressure. Different measurement series are indicated with different markers and colors. Note that during each measurement series, the sample was always kept under pressure, whereas the sample was depressurized between individual measurement series (for example to replace the jacket). The fourth measurement series was performed with two different pore fluid pressures and is divided into two series here. All measurements were performed with a transient pulse of 0.2 MPa over the indicated pore fluid pressure.

4. Discussion

We report 43 permeability measurements performed on a single shale core plug, both when this plug was intact and after it had fractured. Either water or supercritical CO_2 was used as the permeate. The measurements were carried out at either room temperature (between 23 and 25 °C) or at a constant temperature of 40 °C, and at a range of effective confining pressures.

Shale permeability values presented in the literature (e.g., [1,2,19–21]) generally fall in the rather wide range of 10^{-22} - 10^{-15} m^2. Our values fit well within these bounds. In particular, Ghanizadeh et al. [21] report water permeabilities of confined Possidonia shale samples of 1-10 x 10^{-21} m^2, which is very close to our results. The permeability of shale is sensitive to temperature, effective confining pressure, creep, fracturing and microscale damage, and to the permeate (liquid or gas). The effects of these factors, as observed in our experiments, are further discussed in this section.

4.1. Effect of temperature

During the initial measurements, permeability was high and hence measurement duration was short. These measurements could therefore be carried out at room temperature, as room temperature changes (and associated changes in pressure) were too slow to affect the measurements. Further measurements at lower permeability, however, were carried out at a more stable temperature of 40 °C. This value was chosen to ensure that CO_2 would be in its supercritical state. This moderate increase in temperature was assumed to have a negligible (if any) influence on sample permeability. While a direct comparison measurement was note made, this assumption is supported by

the fact that the same permeability was measured before and after the temperature increase (though at different confining pressures).

4.2. Pressure dependence and creep effects

To study the effect of effective confining pressure on shale permeability, the confining pressure was increased in steps between measurements. During the first series of measurements (on a still intact sample plug), permeability decreased with each increase in effective confining pressure as a result of compaction, from 6.6×10^{-18} m^2 at 1.4 MPa to 1.5×10^{-19} m^2 at 12.4 MPa. When the confining pressure was subsequently decreased, the permeability did not recover, and even decreased further to 9.2×10^{-20} m^2 at 2.4 MPa. Similarly, no increase in permeability was observed when comparing the measurement performed at 37.4 MPa effective confining pressure (2.0×10^{-21} m^2) with the subsequent measurement performed at 7.4 MPa effective confining pressure (1.9×10^{-21} m^2). This demonstrates that the observed change in permeability with increasing effective confining pressure is permanent, and not due to elastic effects.

Furthermore, during the first series of measurements, when the effective confining pressure was increased to 12.4 MPa again, a permeability of 4.5×10^{-20} m^2 was measured, lower than before, and the permeability decreased further, to 2.4×10^{-20} m^2 at 17.4 MPa. As compaction continued even when the confining pressure was lower than the maximum applied value, this indicates that at least a part of the compaction was due to time-dependent deformation, i.e. creep, rather than instantaneous plastic deformation. Evidence for such time-dependent deformation was also observed after most pressure increase steps, as significant waiting times (up to several days) were required after each step to allow for the sample to compact and stabilize.

The work of Dong et al. [1] is one of the few existing studies to present pressure-dependent permeabilities of shale. While the permeabilities reported by them are roughly two orders of magnitude higher than those measured here, Dong et al. similarly report that in shale the decrease in permeability with increasing confining pressure is of a permanent nature. They do not discuss any time-dependent component in this change, however. Zhang et al. [2] also report decreasing shale permeability with increasing confining pressure. Sone and Zoback [3] report time-dependent compaction behavior of shale based on mechanical tests. In general, the ductility of shales depends on its total organic carbon and clay contents.

4.3. Effects of fracturing and depressurization

After the initial series of measurements, the confining pressure was further increased to 40 MPa, but no permeability measurement could be carried out due to a leaking jacket. During the replacement of this jacket, the sample split along its bedding (parallel to the sample axis, see Fig. 1). In the second series of measurements, started after the jacket was replaced, at low confining pressure (2.4 MPa) an increased permeability (1.9×10^{-19} m^2) was observed compared to the preceding measurements. However, at higher confining pressure (17.4 MPa), lower permeabilities were measured than before ($5.9 - 8.0 \times 10^{-20}$ m^2). The initially high permeability at low confining pressure was most likely due to increased fluid flow through the fracture. Then, at higher confining pressure, this fracture had “healed” due to compaction of the sample, constricting further fluid flow through the fracture. The lower permeability at an effective confining pressure of 17.4 MPa measured on this core after fracturing compared to the permeability of the core when it was still intact can be explained by the higher effective confining pressure that the sample experienced before fracturing.

An increase in permeability is also observed between the third and fourth series of measurements. This increase was most likely the effect of microscale damage to the sample induced after confining fluid had leaked into the sample (at roughly 40 MPa) and the sample was subsequently very rapidly depressurized to ambient pressure. Interestingly, here the enhanced sample permeability was observed at an effective confining pressure of 17.4 MPa, suggesting that further sample compaction was no longer significant in healing the damage induced in the sample.

4.4. Water vs. CO_2-permeabilities

Three measurements were performed using CO_2 rather than water as the pore fluid. In order to perform these measurements, the sample assembly had to be wrapped with an aluminum foil layer inside the FEP jacket to prevent CO_2-diffusion through the jacket. Unfortunately, the aluminum foil layer in turn negatively impacted the seal of the jacket around the sample, and leakage of confining water into the sample occurred.

All three CO_2-measurements were performed at an effective confining pressure of 17.4 MPa, with supercritical CO_2 at an initial downstream pressure of 7.5 MPa. The first measurement gave a permeability that was 4 times higher than the last preceding measurement performed with water. The second measurement performed with CO_2 gave a permeability that was comparable to the values measured using water. The third measurement gave a permeability that was 3 times lower than the last permeability measured using water.

The initial high permeability may have resulted from damage to the sample induced during depressurization and re-jacketing, it may have resulted from drying of the sample due to exposure to CO_2 and shrinkage of clay minerals, or it may represent a higher permeability of the pore network to CO_2 compared to water. The decreasing permeability in the subsequent measurements may represent sample compaction closing the damage caused by depressurization and re-jacketing or by shrinkage, or, alternatively, it may have been caused by water leaking into the sample. Water inside the sample pores could block such pores to CO_2 flow, thus resulting in a lower permeability, or the re-entry of water into the sample may have caused the expansion of clay minerals, reducing sample permeability. To distinguish what effects caused the decreasing permeability of the sample when using CO_2, further measurements are therefore required.

Bloomfield and Williams [22] report a difference of up to two orders of magnitude between gas and liquid permeabilities measured on sandstone and shale samples, which they attribute to the Klinkenberg effect [23]. Tanikawa and Shimamoto [24] similarly report up to one order of magnitude difference between gas and liquid permeabilities measured on sandstones. Their calculations show that this difference can be ascribed to the Klinkenberg effect. Dong et al. [1] estimate that in their experiments, the Klinkenberg effect only influenced the measured permeabilities by less than one order of magnitude. The initial increase in permeability observed in our CO_2-measurements thus falls within the range of the Klinkenberg effect observed by other authors, and can be explained by this effect. Ghanizadeh et al. [21] report a difference of up to three orders of magnitude between water and gas (He and CH_4) permeabilities in Possidonia shale, which they attribute to thin films of structured water on mineral surfaces and/or the enhanced compaction of the samples upon introduction of water.

5. Summary and conclusions

Based on 43 permeability measurements performed on a single, confined plug of Rurikfjellet formation shale, using either water or CO_2 as the permeate, we report the following observations:

- Sample permeability decreased with increasing effective confining pressure. This decrease in permeability was largely permanent (i.e., not due to elastic deformation).
- Permeability changes were also time-dependent, demonstrating compaction by creep.
- At elevated effective confining pressure (17.4 MPa), a fracture through our sample (parallel to bedding and to the sample axis) did not influence the measured permeability, suggesting that the fracture had effectively closed due to compaction and healing at an effective confining pressure in excess of 2.4 MPa.
- The measured CO_2-permeabilities were similar to the water permeability, but more measurements are required here.

Acknowledgements

This research was funded by Gassnova, UNIS CO_2 Lab, and FME SUCCESS (grant 193825/S60 from the Research Council of Norway). The authors also wish to thank Sven Vangbæk of the NGI for preparing the sample plug used.

References

[1] Dong J-J, Hsu J-Y, Wu W-J, Shimamoto T, Hung J-H, Yeh E-C, Wu Y-H, Sone H. Stress-dependence of the permeability and porosity of sandstone and shale from TCDP Hole-A. Int J Rock Mech Min 2010;47:1141-1157.

[2] Zhang R, Ning Z, Yang F, Zhao H, Wang Q. A laboratory study of the porosity-permeability relationships of shale and sandstone under effective stress. Int J Rock Mech Min 2016;8:19-27.

[3] Sone H, Zoback MD. Time-dependent deformation of shale gas reservoir rocks and its long-term effect on the in situ state of stress. Int J Rock Mech Min 2014:69;120-132.

[4] Yarushina VM, Bercovici D, Oristaglio ML. Rock deformation models and fluid leak-off in hydraulic fracturing. Geophys J Int 2013;194:1514-1526.

[5] Räss L, Yarushina VM, Simon NSC, Podladchikov YY. Chimneys, channels, pathway flow or water conducting features - an explanation from numerical modelling and implications for CO_2 storage. Energy Procedia 2014;63:3761-3774.

[6] Skurtveit E, Aker E, Soldal M, Angeli M, Wang Z. Experimental investigation of CO_2 breakthrough and flow mechanisms in shale. Petrol Geosci 2012;18:3-15.

[7] Verdon JP, Kendall JM, Stork AL, Chadwick RA, White DJ, Bissell RC. Comparison of geomechanical deformation induced by megatonne-scale CO_2 storage at Sleipner, Weyburn, and In Salah. P Natl Acad Sci 2013;110:E2762-E2771.

[8] Alemu BL, Aagaard P, Munz IA, Skurtveit E. Caprock interaction with CO_2: A laboratory study of reactivity of shale with supercritical CO_2 and brine. Appl Geochem 2011;26:1975-1989.

[9] Credoz A, Bildstein O, Jullien M, Raynal J, Pétronin JC, Lillo M, Pozo C, Geniaut G. Experimental and modeling study of geochemical reactivity between clayey caprocks and CO_2 in geological storage conditions. Energy Procedia 2009;1:3445-3452.

[10] Ilton ES, Schaef HT, Qafoku O, Rosso KM, Felmy AR. In Situ X-ray Diffraction Study of Na^+ Saturated Montmorillonite Exposed to Variably Wet Super Critical CO_2. Envir Sci Tech 2012;46:4241-4248.

[11] Schaef HT, Ilton ES, Qafoku O, Martin PF, Felmy AR, Rosso KM. *In situ* XRD study of Ca^{2+} saturated montmorillonite (STX-1) exposed to anhydrous and wet supercritical carbon dioxide. Int J Greenh Gas Con 2012;6:220-229.

[12] De Jong SM, Spiers CJ, Busch A. Development of swelling strain in smectite clays through exposure to carbon dioxide. Int J Greenh Gas Con 2014;24:149-161.

[13] Braathen A, Bælum K, Christiansen HH, Dahl T, Eiken O, Elvebakk H, Hansen F, Hanssen TH, Jochmann M, Johansen TA, Johnsen H, Larsen L, Lie T, Mertes J, Mørk A, Mørk MB, Nemec W, Olaussen S, Oye V, Rød K, Titlestad GO, Tveranger J, Vagle K. The Longyearbyen CO_2 Lab of Svalbard, Norway—initial assessment of the geological conditions for CO_2 sequestration. Norw J Geol 2012;92:353-376.

[14] Iden K. Longyearbyen CO_2-lab-core petrography, IFE Report no. IFE/KR/F-2012/136, IFE; 2012.

[15] Brace WF, Walsh JB, Frangos WT. Permeability of granite under high pressure. J Geophys Res 1968;73:2225:2236.

[16] Zoback, MD, Byerlee JD. The effect of microcrack dilatancy on the permeability of Westerly granite. J Geophys Res 1975;80:752-755.

[17] Firouzi M, Alnoaimi K, Kovscek A, Wilcox J. Klinkenberg effect on predicting and measuring helium permeability in gas shales. Int J Coal Geol 2014;123:62-68.

[18] Wagner W. FLUIDCAL, Software for the calculation of thermodynamic and transport properties of a great number of fluids, Bochum: Ruhr-Universität Bochum; 2014.

[19] Chalmers GRL, Ross DJK, Bustin, RM. Geological controls on matrix permeability of Devonian Gas Shales in the Horn River and Liard basins, northeastern British Columbia, Canada. Int J Coal Geol 2012;103:120-131.

[20] Chalmers GRL, Bustin RM. Geological evaluation of Halfway-Doig-Montney hybrid gas shale-tight gas reservoir, northeastern British Columbia. Mar Petrol Geol 2012;38:53-72.

[21] Ghanizadeh A, Amann-Hildenbrand A Gasparik M, Gensterblum Y, Krooss BM, Littke R. Experimental study of fluid transport processes in the matrix system of the European organicrich shales: II. Posidonia Shale (Lower Toarcian, northern Germany), Int J Coal Geol 2014;123:20-33.

[22] Bloomfield JP, Williams AT. An empirical liquid permeability-gas permeability correlation for use in aquifer properties studies. Q J Eng Geol 1995;28:S143-S150.

[23] Klinkenberg LJ. The permeability of porous media to liquids and gases. SOCAR Proceedings 1941;2:200-213.

[24] Tanikawa W, Shimamoto T. Comparison of Klinkenberg-corrected gas permeability and water permeability in sedimentary rocks, Int J Rock Mech Min 2009;46:229-238.